Science and Technology of Advanced Materials

ISSN: 1468-6996 (Print) 1878-5514 (Online) Journal homepage: www.tandfonline.com/journals/tsta20

Sustainable and robust biomass-based binder for silicon anodes in lithium-ion batteries: cross-linked sodium alginate and chondroitin sulfate

Hyun Wook Jung, Seung Min Ko & Jung Tae Lee

To cite this article: Hyun Wook Jung, Seung Min Ko & Jung Tae Lee () Sustainable and robust biomass-based binder for silicon anodes in lithium-ion batteries: cross-linked sodium alginate and chondroitin sulfate, Science and Technology of Advanced Materials, just-accepted:just-accepted, 2523243, DOI: 10.1080/14686996.2025.2523243

To link to this article: https://doi.org/10.1080/14686996.2025.2523243

Accepted author version posted online: 30 Jun 2025.

Publisher: Taylor & Francis & The Author(s). Published by National Institute for Materials Science inpartnership with Taylor & Francis Group.
Journal: *Science and Technology of Advanced Materials*
DOI: 10.1080/14686996.2025.2523243

Sustainable and Robust Biomass-Based Binder for Silicon Anodes in Lithium-Ion Batteries: Cross-linked Sodium Alginate and Chondroitin Sulfate

Hyun Wook Jung [a,1], *Seung Min Ko* [a,1] *and Jung Tae Lee* [a,*]

[a] Department of Convergent Biotechnology and Advanced Materials Science, Kyung Hee University, 1732, Deogyeong-daero, Giheung-gu, Yongin-si, Gyeonggi-do, 17104, Republic of Korea

* Corresponding authors

E-mail addresses: J.T.Lee (jungtae@khu.ac.kr)

[1] These authors contributed equally to this work

Keywords: Silicon anode, cross-linking, binder, eco-friendly, biomass

Abstract

Silicon (Si) is a promising next-generation anode material for lithium-ion batteries (LIBs) due to its exceptionally high theoretical capacity (3579 mAh g^{-1}) and natural abundance. However, its commercialization remains challenging due to severe volume expansion (~300%) during cycling, leading to poor structural stability and rapid capacity degradation. To address this issue, we developed a novel biomass-derived binder system denoted as SCC, composed of sodium alginate (SA) and chondroitin sulfate (CS), crosslinked via a simple calcium chloride ($CaCl_2$) aqueous treatment. Unlike conventional synthetic polymer-based binders, this system enhances mechanical stability while maintaining an environmentally friendly, water-based fabrication process. Spectroscopic analysis confirmed strong hydrogen bonding interactions between SA and CS, as well as robust crosslinking formation through Ca^{2+}. These interactions effectively enhance the mechanical strength of the SCC binder, enabling it to accommodate the severe volume changes that occur during electrochemical reactions in Si anodes. This, in turn, contributes to enhanced structural stability of Si electrode, which leads to a reduction in both solid electrolyte interphase and charge transfer resistance. As a result, the SCC electrode showed improved electrochemical cycling stability, with a 13.45% higher capacity retention after 60 cycles at a 0.2C rate compared to SA alone. This suggests its potential as a sustainable and scalable solution for next-generation high-performance Si anodes.

1. Introduction

Lithium-ion batteries (LIBs) have become an indispensable energy storage solution for portable electronic devices and electric vehicles in the modern era. With the progression of time, the demand for energy has increased, leading to a corresponding rise in the energy density required for LIBs [1-3]. To address this, extensive research has been conducted on electrode materials for LIBs, resulting in significant improvements in energy density [4-6]. However, the commercialized anode materials currently in use, such as graphite, hard carbon, and lithium titanate oxide ($Li_4Ti_5O_{12}$), still have limited theoretical reversible capacities [7-9]. In an effort to replace these anode materials with constrained theoretical capacities, silicon (Si) has been extensively studied due to its high theoretical gravimetric capacity (3579 mAh g^{-1} for $Li_{3.75}Si$) and its abundance in the Earth's crust. Additionally, Si is considered a promising next-generation anode material because of its low cost and eco-friendly properties [10,11]. Despite these advantages, Si anodes face significant barriers to commercialization due to their inherent characteristics. Specifically, the severe volume expansion of approximately 300% during charge-discharge cycles leads to phenomena such as pulverization of Si, delamination of active material, and the repeated destruction and regeneration of the solid electrolyte interphase (SEI). These phenomena contribute to mechanical and electrical failure of the electrode structure, as well as continuous lithium-ion consumption during long-term cycling, ultimately resulting in irreversible capacity loss and a dramatic reduction in cycling stability [12,13].

Over the past decade, research has focused on material engineering to create new active materials by nanostructuring methods such as nanowires and nanotubes, or by oxidation, such as SiO_2, to address the persistent issues with Si [11]. Alongside this, binder materials that can

mechanically stabilize and secure electrode materials have become an essential research area to overcome the limitations of Si anodes. Poly(vinylidene fluoride) (PVDF), widely used in commercial LIBs, faces challenges due to its weak mechanical strength, making it unsuitable for Si anodes [14]. As a result, there has been increased research into binders with stronger mechanical properties. In particular, binders that utilize crosslinking to enhance mechanical strength have gained attention as an effective solution to accommodate Si's volume expansion. For instance, Ye, Ruilai, et al. created a structured binder through crosslinking by combining poly(acrylic acid), gelatin and β-cyclodextrin, and Wang, Hongxun, et al. developed a 3D network crosslinked binder that forms strong covalent bonds by using sodium hyaluronate and epichlorohydrin [15,16]. These crosslinking-based binders, which form a network structure between polymer chains, enable the binder to more effectively secure the electrode and withstand the mechanical stress caused by the volume changes of silicon, thereby exhibiting strong mechanical properties and significantly improving the cycling stability of Si anodes. However, many of these crosslinked binders contain synthetic polymers or crosslinking agents made from synthetic materials, leading to environmentally unfriendly processes that often involve the use of organic solvents or toxic substances.

In this study, we present a novel binder composed solely of biomass-derived polymers designed to provide suitable mechanical strength for Si anodes. Biomass, unlike synthetic materials, refers to renewable organic materials such as plants, animals, algae, and microorganisms. As a sustainable resource, biomass offers abundant availability and easy access to raw materials, significantly reducing production costs. Therefore, it holds great promise as a low-cost and eco-friendly alternative in various material applications [17]. In light of these characteristics, we developed the binder by mixing sodium alginate (SA) with chondroitin sulfate (CS) and crosslinked it using a simple coating of a calcium chloride

($CaCl_2$) aqueous solution, thereby enhancing the electrode structure and mechanical strength of the binder, denoted as SCC. SA is a major component of brown algae and possesses a copolymer structure composed of 1→4 linked β-D-mannuronic acid (M) and α-L-guluronic acid (G) residues. SA has been widely applied as a binder in various electrode materials, and it has been reported to exhibit excellent performance when used alone as a binder for Si anodes [18-21]. Therefore, the goal of this study is to enhance its performance by incorporating SA with CS, a combination that has not yet been explored in the field of Si anode binders. CS is a natural polymer primarily found in the skeletal structures of animals and belongs to the glycosaminoglycan (GAG) family of complex heteropolysaccharides. It is characterized by the presence of sulfate groups in varying numbers and positions and has a structure in which glucuronic acid (GlcA) and N-acetyl-D-galactosamine (GalNAc) are linked via β (1→3) bonds [22]. Unlike previously reported crosslinked binders, this binder exclusively utilizes biomass-derived polymers, and the crosslinking agent is a non-toxic substance, making the process environmentally friendly [23-25]. We confirmed the interaction between SA and CS via hydrogen bonding and crosslinking of the SCC on the Si anode. These interactions, including both hydrogen bonding and crosslinking, effectively enhance the mechanical strength of the SCC, enabling it to accommodate the severe volume changes that occur during electrochemical reactions in Si anodes compared to the simple SA-based electrode. Importantly, the SCC is composed of SA and CS, both of which are water-soluble natural polymers derived from sustainable biomass sources. And additionally, the system utilizes a non-toxic $CaCl_2$ aqueous solution. The overall electrode fabrication process can be carried out using an eco-friendly, water-based approach rather than organic solvents, thereby minimizing hazardous emissions and improving environmental safety. The development of this environmentally benign SCC contributes to ongoing efforts in the field of silicon anode binders, further supporting the potential of natural polymer-based, high-

performance binders.

2. Materials & methods

Materials

Ethylene carbonate (EC), diethyl carbonate (DEC), lithium hexafluorophosphate ($LiPF_6$), sodium alginate (SA, molecular weight: 120,000-190,000 g/mol), and calcium chloride anhydrous ($CaCl_2$) were purchased from Sigma-Aldrich Co. (Korea). SUPER C65 (Super C), a conductive carbon, was purchased from MTI Co. (Korea). Fluoroethylene carbonate (FEC) and vinylene carbonate (VC) were purchased from Thermo-Scientific Co. (Korea). Polyvinylidene fluoride (PVDF) was purchased from Arkema Co. (Korea). Chondroitin sulfate sodium salt (CS, molecular weight: 1000 g/mol) was purchased from TCI Co. (Korea). Nano silicon particles (Si, 50-80 nm) were purchased from Skyspring-Nanomaterials Co. (USA).

Preparation of Electrodes

The fabrication of electrodes involved the preparation of slurries containing active materials, binders, and conductive additives. For the SC electrode (SC/Si), a slurry was prepared by mixing nano-Si, a 5 wt% SC aqueous solution (weight ratio, SA:CS = 1:9), and Super C65 in a ratio of 6:2:2 (Si : SC : Super C65), and cast onto a copper foil using a doctor blade with a gap of 100 μm. For the SCC electrode (SCC/Si), after drying the previously fabricated SC electrode at room temperature for 30 minutes, a 1 wt% $CaCl_2$ aqueous solution prepared in distilled water (DW) was applied to the same electrode. Subsequently, the SC and SCC electrode was dried in a vacuum oven at 100 °C for 12 hours. The SA electrode (SA/Si) was

prepared by mixing Si, a 5 wt% SA aqueous solution, and Super C65 in the same 6:2:2 ratio (Si : SA : Super C65). The resulting slurry was cast onto a copper foil using a doctor blade with a gap of 100 μm and dried in a vacuum oven at 100 °C for 12 hours. The PVDF electrode (PVDF/Si) was prepared by a 5 wt% PVDF in NMP solution, The subsequent composition ratios and fabrication procedures are identical to those used for the other electrode preparation methods. The areal loading of all electrodes was 1.0~1.2 mg cm^{-2}.

Material Characterization

Fourier Transform Infrared Spectroscopy (FT-IR, Thermo Scientific Nicolet iS10) was employed to analyze the molecular interactions and functional groups present in the SA, SC, and SCC films. The measurements were conducted with a resolution of 1 cm^{-1} over the spectral range of 400 to 4000 cm^{-1} using 16 scans per sample. For the surface analysis of the electrodes, X-ray photoelectron spectroscopy (XPS, K-Alpha, Thermo Electron) was used with an Al Kα X-ray source under high vacuum conditions, with a spot size of 400 μm^2. Field-Emission Scanning Electron Microscopy (SEM, LEO SUPRA 55, GENESIS 2000) was conducted to examine the surface morphology of the electrodes. Tensile strength tests were performed to evaluate the mechanical properties of the pure SA, SC, and SCC films using a Texture Analyzer (CT3 25 K, Brookfield) with a test speed of 0.20 mm/s. Peeling tests were conducted to assess the adhesion properties of the binders, determining their ability to maintain contact with the electrode materials under stress using a Texture Analyzer. A 12 mm × 20 mm adhesive tape was applied to the electrode surface, and the peeling force was measured accordingly. Thin films of SA, CS, SC, and SCC were prepared by casting their respective solutions into a 4 × 4 cm^2 square mold, with SA at 5 wt% and CS, SC and SCC at 10 wt% in DW, to achieve a uniform thickness of 10 μm. Dog-bone specimens were prepared

from the thin films with dimensions of 22mm in length and 2 mm in width for tensile strength tests.

Electrochemical Characterization

CR2032 coin cells were assembled in an argon-filled glove box (MOTEK, O_2 and H_2O < 0.5 ppm) to analyze the electrochemical properties of the Si anode with different binders. Celgard 2400 and a Li metal foil were used as the separator and anode, respectively. The electrolyte was 1 M $LiPF_6$ in an EC/DEC solution (1:1, v/v) with the addition of 10 wt% FEC and 1 wt% VC. The electrolyte/Si (E/Si) ratio was 30 μL mg^{-1}. In the galvanostatic experiments, Galvanostatic charge-discharge (GCD) and cycle tests were conducted using the NMW-200-160CH (NEWARE) equipment, whereas. Potentiostat tests (cyclic voltammetry (CV) and EIS) were performed using CV ZIVE sp1 (WonATech) equipment. Two formation cycles were performed at a voltage range of 0.005 V to 1.5 V at 0.05 C, followed by GCD tests conducted within a voltage range of 0.01-1.0 V for each current density. The formation cycles were conducted at a range of 0.005 V to 1.5 V at 0.05 C and 0.2 C for one cycle each, followed by subsequent cycles at a range of 0.01 V to 1.0 V at 0.2 C. The CV analysis of SCC cells was conducted in the range of 0.001-1.5 V at 0.1 mV s^{-1}. EIS was scanned with an AC voltage amplitude of 0.01 mV between 100 kHz and 0.1 Hz.

3. Results and discussion

3.1. Synthesis and characterization of SCC

The comprehensive experimental procedure for fabricating the SCC is illustrated in Figure 1(a). To synthesize the final SCC, SA and CS were initially dissolved in DW and subsequently mixed to prepare the SC solution. SA is a naturally occurring polysaccharide composed of β-D-mannuronic acid (M) and α-L-guluronic acid (G) residues linked in a copolymeric structure (Figure S1(a)). This biopolymer is characterized by a high density of polar functional groups, including hydroxyl (–OH) and carboxyl (–COOH) moieties, which facilitate intermolecular interactions. Similarly, CS, a naturally derived polysaccharide consisting of GlcA and GalNAc linked via β (1→3) glycosidic bonds, exhibits a diverse array of polar functional sites, including –OH groups, sulfate groups ($–OSO_3^-$), and N–H bonding regions (Figure S1(b)). Given their inherent polarity, SA and CS possess significant potential for intermolecular hydrogen bonding interactions. To experimentally validate these interactions, thin films of each material were fabricated and analyzed via FTIR spectroscopy, as depicted in Figure 1(b). A broad absorption band consistently observed at 3320 cm^{-1} across all samples corresponds to the stretching vibrations of O–H bonding. The FTIR spectrum of the pure SA film prominently features a peak at 1297 cm^{-1}, which is attributed to C–C–H and O–C–H deformations within pyranose ring structures [18]. While the spectral features of the pure CS film largely resemble those of SA due to the inherent structural similarities of polysaccharides, a distinct peak at 1222 cm^{-1}, attributed to $–OSO_3$, differentiates the two spectra. In the spectrum of the SC film, examining the peaks attributed to the glycosidic rings in the range of 1100 cm^{-1} to 950 cm^{-1} reveals that the peak for SA film is observed at 1021.36

cm^{-1}, while for CS film, it is observed at 1028.91 cm^{-1} (Figure S2) [26,27]. In contrast, the SC film shows the peak at 1022.78 cm^{-1}, which can be interpreted as an intermediate wavenumber resulting from the superimposition of the C–O–C peaks of the two polymers. These findings demonstrate the spectral contributions of both SA and CS within the SC film. Overall, it is evident that both SA and CS exert significant influence on the structure of the SC film.; however, a crucial observation is the pronounced reduction in the relative intensity of the 1300 cm^{-1} peak. Given that this vibrational mode corresponds to C–C–H and O–C–H deformations in the pyranose ring structure of the SA monomer, its attenuation suggests that the incorporation of CS induces structural modifications via intermolecular hydrogen bonding interactions. This finding provides compelling evidence of chemical interactions occurring within the SC mixture, as similarly discussed in previous studies [18].

To investigate the potential interactions between SA, CS, and Si when used as a binder matrix for Si anodes, XPS analysis was performed (Figure 1(c)). The Si 2*p* spectra of pure Si particles (Si/C) and those mixed with SA and CS (Si/C/SC) revealed an increase in the binding energy corresponding to Si–O bonding. This shift is attributed to hydrogen bonding interactions between the native oxide layer on the Si surface and the –OH groups inherently present in SA and CS. Such interactions may contribute to mitigating the pulverization of Si caused by volume expansion during cycling, thereby enhancing the long-term stability of Si anodes [28,29]. To further enhance the crosslinking efficacy of the SCC, Ca^{2+} ions were introduced as crosslinking agents. The incorporation of Ca^{2+} was accomplished through a straightforward yet effective method, wherein a slurry containing SC solution, Si, and carbon was first cast to obtain the electrode, followed by the application of an aqueous $CaCl_2$ solution onto the electrode surface. The extent of the resultant crosslinking reaction was subsequently assessed through XPS analysis. To evaluate whether crosslinking between the two natural polymers, SA and CS, occurs successfully upon the introduction of $CaCl_2$ into the

SA–CS matrix, a comparative analysis of the C 1*s* and S 2*p* spectra of SC and SCC films was conducted (Figure S3). XPS analysis focused on anionic functional groups—specifically carboxyl and sulfate groups—which are considered potential sites for crosslinking. After crosslinking, the carboxyl group exhibited a clear shift in binding energy, indicating a successful ionic exchange of Na^+ with Ca^{2+} and the subsequent formation of crosslinked structures (Figure S3(a)) [30]. In contrast, the sulfate group showed no significant change in binding energy before and after crosslinking, suggesting that it does not participate in the crosslinking reaction (Figure S3(b)). These findings confirm that the crosslinking in the SCC matrix predominantly occurs through interactions between carboxyl groups, and a corresponding crosslinking model is proposed in Figure S4. Finally, to determine whether Ca^{2+} ions effectively participated in crosslinking within the SCC/Si when introduced via a simple coating of $CaCl_2$ solution onto the SC/Si, Ca 2*p* spectra were examined. This analysis was performed both before and after ethanol washing of the SCC/Si following the crosslinking treatment. In both cases, the resulting spectrum exhibited two characteristic peaks at 347.58 eV and 351.13 eV, corresponding to Ca $2p_{3/2}$ and Ca $2p_{1/2}$, respectively (Figure 1(d)), which are attributed to Ca–O bonding formed as a result of the crosslinking reaction. These results demonstrate that even a straightforward $CaCl_2$ aqueous solution coating can induce effective crosslinking. Collectively, the observed binding energy shift of the carboxyl peak in the C 1*s* spectra of the SCC film and electrode, along with the Ca–O bonding signal in the Ca 2*p* spectra, provide direct evidence that Ca^{2+} ions facilitate crosslinking through interactions with carboxyl groups. This finding is consistent with previous literature reports [31].

Collectively, these findings demonstrate that the SCC undergoes effective crosslinking within the electrode matrix through a facile yet robust fabrication process, thereby enhancing the

adhesion of electrode materials. The overall schematic representation of this process is depicted in Figure 1(a).

3.2. Mechanical properties and surface morphology of SCC/Si

To elucidate the morphological and structural evolution of Si anodes as a function of binder composition, electrodes were fabricated and analyzed via SEM imaging, as presented in Figure 2(a–c). The top-view SEM image of the SA/Si (Figure 2(a)) reveals a highly porous three-dimensional (3D) network, characteristic of its intrinsic polymeric structure. This morphology arises from the fundamental nature of SA, a biopolymer composed of M and G residues. Polysaccharides derived from biomass frequently exhibit copolymeric architectures, wherein diverse monomeric units coexist within a single polymer backbone. Such structural complexity has been reported to induce a porous framework when employed as a binder, a phenomenon attributed to the inherent heterogeneity of molecular interactions [32,33]. In contrast, the SC/Si (Figure 2(b)) exhibits a denser and more homogeneous morphology. This transition is ascribed to the incorporation of CS, which modifies the interpolymeric interactions within the binder system. The introduction of CS imparts additional functional groups, including $-OSO_3^-$ and -OH, which engage in intermolecular interactions with the -COOH and -OH of SA. The resulting semi-interconnected network mitigates the inherent aggregation tendency of SA, thereby promoting a more uniform electrode architecture. A key observation is derived from the top-view SEM images of electrodes with varying SA-to-CS ratios, as presented in Figure S5. Despite the gradual increase in CS content within the SA matrix, the electrode morphology remains largely similar to that of the SA/Si up to a SA:CS weight ratio of 1:5. This indicates that SA plays a dominant role in determining the non-uniform structural framework of the electrode. Such non-uniform electrode structures may

serve as sites of localized stress caused by the repeated volume expansion of aggregated Si particles, potentially leading to mechanical failure over extended cycling [34]. Therefore, in this study, the SA-to-CS ratio was optimized to 1:9 wt%, which resulted in a more uniform electrode structure. This optimized composition was adopted for all subsequent analyses. The SCC/Si (Figure 2(c)) demonstrates an even more compact morphology, though minor agglomeration is observed. This structural evolution is attributed to the incorporation of Ca^{2+}, which act as crosslinking agents, further reinforcing interactions between SA and CS. During electrode fabrication, Ca^{2+} coordinate with the carboxyl moieties of SA and CS, facilitating the formation of a robust crosslinked network. Despite the enhanced cohesion imparted by ionic crosslinking, the SCC/Si does not exhibit the pronounced aggregation observed in the SA/Si. This is due to the sequential processing approach, wherein Ca^{2+} is introduced post-electrode formation via aqueous solution coating. Consequently, the final electrode morphology remains well-defined and structurally coherent.

Si undergoes an intrinsic alloying reaction during lithiation/delithiation, resulting in severe volumetric expansion, which poses a significant challenge to electrode integrity. Consequently, the binder for Si anodes must exhibit exceptional mechanical robustness to accommodate these volumetric fluctuations. To assess whether SCC, when employed as a binder, can effectively preserve the structural integrity of the Si anode over multiple cycles, the tensile strength of the pristine binder films was first evaluated, as presented in Figure 2(d) and Figure S6(a). The SA and CS film exhibited a tensile strength of 150.92 MPa and 123.21 MPa, indicating relatively weak mechanical properties. In contrast, the SC film demonstrated an improved tensile strength of 178.36 MPa, which can be attributed to the formation of a semi-interconnected network reinforced by intermolecular hydrogen bonding between SA and CS. However, the absence of ionic crosslinking limits its ability to achieve greater mechanical integrity. Notably, the SCC film exhibited a dramatic enhancement in mechanical

strength, reaching a tensile strength of 394.94 MPa. This substantial improvement is primarily ascribed to the incorporation of Ca^{2+} ions, which facilitate ionic crosslinking with the -COOH of SA and CS, thereby reinforcing the binder matrix. These findings are further corroborated by the Young's modulus values presented in Figure 2(e), where a progressive increase is observed from SA film (0.0539 GPa) to SC film (0.0654 GPa), with SCC film reaching the highest modulus of 0.1202 GPa. Notably, CS film exhibits a higher Young's modulus of 0.082 GPa compared to both SA and SC film, which, despite its lower tensile strength, reflects the intrinsic brittleness of CS (Figure S6(b)). This explains the increase in modulus observed in the SC film relative to SA upon the incorporation of CS. Ultimately, the highest modulus observed in the SCC film underscores the critical role of crosslinking in enhancing the structural integrity of the binder matrix, with SCC film exhibiting superior stiffness and mechanical stability compared to SA and SC film. To assess whether SCC, when introduced as a binder, significantly contributes to improving the mechanical properties of the electrode, a peeling test was conducted using electrodes intended for actual electrochemical measurements (Figure S7). The averaged peeling force presented in Figure 2(f) and Figure S8 reveals that SA/Si and CS/Si exhibits relatively low values, whereas a gradual increase is observed from the SC/Si to the SCC/Si. This trend suggests that the reinforced polymeric interactions previously discussed effectively enhance adhesion within the electrode, securing active materials more efficiently. Such improvements in mechanical properties are crucial for enduring the cyclic stress induced by Si's volumetric expansion, thereby ensuring the long-term structural integrity of the electrode.

3.3. Electrochemical performance of the SCC/Si

The ability of SCC to preserve electrode integrity is further corroborated by its electrochemical performance. Before evaluating the cycling performance of the electrodes with different binders, the initial coulombic efficiency (ICE) of each electrode was examined (Figure S9). The PVDF/Si using the widely adopted commercial binder PVDF exhibited an ICE of 86.62%, while the SA/Si showed 89.81%, and the SCC/Si demonstrated the highest ICE of 89.94%. This improvement is attributed to the previously discussed electrode structure and the superior mechanical properties provided by the crosslinked structure of SCC, which helps maintain electrode integrity during the initial lithiation process and minimizes lithium-ion consumption caused by repeated SEI formation. As shown in the cycling data at a 0.2C rate (Figure 3(a)), the PVDF/Si initially delivers a capacity of 2606 mAh g^{-1}; however, rapid capacity degradation is observed from the early cycles. This decline is attributed to the pulverization of Si particles due to severe volumetric expansion, leading to a loss of active material, continuous solid electrolyte interphase (SEI) reformation consuming Li^+, and delamination of active material from the current collector. As observed in the GCD profiles extracted from the cycling data, the capacity retention of the PVDF/Si drops to 21.71% after the 60th cycle, further highlighting the inherent limitations of PVDF as a binder for Si anodes (Figure S10). The SA/Si exhibits an initial capacity of 3067 mAh g^{-1} and demonstrates better capacity retention compared to PVDF; however, a gradual decline in capacity is observed from the early cycles. In contrast, the SCC/Si exhibits an initial capacity of 3171 mAh g^{-1}, comparable to SA/Si, but crucially, no substantial capacity loss is observed in the early cycles. This stability suggests that the tailored structure of SCC effectively accommodates Si's volumetric fluctuations during cycling. The distinction between the two systems is

further evident in their GCD profiles (Figure 3(b, c)). By the 20th cycle, the SA/Si (Figure 3(b)) exhibits a capacity fade of approximately 200 mAh g^{-1}, with continuous degradation in subsequent cycles. Conversely, the SCC/Si (Figure 3(c)) maintains a capacity nearly identical to its initial value through the 20th cycle, with this trend persisting up to the 40th cycle. By the 60th cycle, the SA/Si retains only 64.97% of its initial capacity, whereas the SCC/Si retains 73.71%, showing relatively better reversibility. To determine whether the enhanced capacity retention of the SCC/Si arises from electrochemical contributions of the binder itself, CV measurements were conducted. The SCC/Si exhibits characteristic oxidation and reduction peaks associated with Si-Li alloying reactions, with no additional redox activity detected [35]. This confirms that SCC does not undergo electrochemical reactions within the tested voltage window, reinforcing the conclusion that its superior cyclability and capacity retention stem from its enhanced mechanical properties, which effectively sustain Si anode integrity.

To further investigate the influence of each binder on Si anode electrochemical behavior under increased current densities, rate capability tests were conducted (Figure 3(e)). Notably, SCC/Si exhibits a significant capacity advantage over SA/Si at moderate rates up to 0.5C. However, as the rate increases, the capacity gap between SCC/Si and SA/Si narrows. This behavior is reflected in their respective voltage profiles (Figure 3(f, g)), where polarization differences remain minimal across increasing current densities. Interestingly, at 2C, the plateau voltage of SA/Si is slightly higher than that of SCC/Si. This phenomenon can be rationalized based on the structural characteristics of the SA/Si. As previously confirmed, the SA/Si exhibits a more porous macroscopic morphology compared to SCC/Si, which may facilitate enhanced electrolyte infiltration. Under high current density conditions, where mass transport becomes the dominant factor, the inherently porous architecture of SA/Si provides a kinetic advantage [33]. However, a critical limitation of SA/Si remains—its inherently weak

mechanical strength and non-uniform morphology, which lead to localized expansion stress points and severe active material degradation. This is further evidenced in Figure 3(f, g), where despite SA/Si exhibiting stable polarization behavior at high rates, its lithiation capacity remains inferior to SCC/Si due to persistent active material loss. This trend is further corroborated by the capacity recovery observed when the SCC/Si, after being cycled at a high rate of 2C, is returned to a lower rate of 0.2C, demonstrating its ability to regain capacity effectively (Figure S11).

3.4. Post-cycled analysis of the SCC/Si

To evaluate the extent to which electrode integrity is maintained after cycling, given the enhanced mechanical durability of the SCC, post-cycling analyses were performed. Specifically, the resistance of SA/Si and SCC/Si after the 5th and 60th cycles were assessed using Nyquist plots obtained from EIS measurements (Figure 4(a, b)). After the 5th cycle, both SA/Si and SCC/Si exhibited comparable resistance values, with SCC/Si showing a slightly lower resistance. However, after 60 cycles, the SCC/Si demonstrated a noticeably lower resistance than SA/Si, indicating its improved ability to retain structural integrity under repeated lithiation/delithiation cycles.

To further analyze the individual resistance components in the Nyquist plots, the data were fitted to an equivalent circuit model (Figure S12) (Figure 4(c)). The results showed that in the SA/Si, the SEI resistance (R_{SEI}) increased from 13.451 Ω at the 5th cycle to 164.127 Ω after 60 cycles, while the charge transfer resistance (R_{ct}) rose from 44.835 Ω to 230.892 Ω. In contrast, the SCC/Si exhibited a more moderate increase, with R_{SEI} increasing from 4.709 Ω to 86.837 Ω and R_{ct} from 28.769 Ω to 171.644 Ω. During repeated lithiation and delithiation cycles, Si particles undergo severe volume expansion and contraction. If the mechanical strength of the surrounding binder material is insufficient, the Si particles become highly susceptible to pulverization. This process exposes fresh Si surfaces, leading to the continuous formation and reconstruction of the SEI as the pre-existing SEI fractures and reforms [36]. Consequently, the progressive thickening of the SEI layer results in increased resistance. Furthermore, the repeated volumetric fluctuations of numerous Si particles during cycling induce significant structural defects within the electrode, ultimately compromising the

integrity of the continuous electrode matrix. This structural degradation disrupts the conductive pathways within the electrode, thereby increasing charge transfer resistance [37,38]. The fact that the SCC/Si exhibits a smaller increase in both R_{SEI} and R_{ct} after 60 cycles compared to the SA/Si demonstrates that the designed structure, coupled with the enhanced mechanical properties of the SCC, effectively preserves the integrity of both the Si particles and the electrode framework.

The post-cycling analysis of SA/Si and SCC/Si was further conducted through SEM imaging, allowing for direct visual inspection. The top-view SEM image of the post-cycled SA /Si (Figure 4(d)) reveals the presence of major crack throughout the electrode. This indicates that the insufficient mechanical strength of the SA fails to adequately preserve the structural integrity of the Si anode during cycling. In contrast, the top-view SEM image of the SCC/Si (Figure 4(e)) shows the presence of minor cracks induced by cycling; however, the overall electrode integrity appears to be better maintained compared to the SA /Si. These observations align with the differences in resistance values obtained from EIS measurements, further supporting that the mechanically reinforced structure of the SCC—achieved through cross-linking via SA, CS, and $CaCl_2$ aqueous solution coating—effectively mitigates the structural degradation of the Si anode.

4. Conclusions

In this study, we developed a novel biomass-derived binder system tailored for Si anodes in LIBs, addressing the critical challenges posed by Si's severe volumetric expansion during cycling. The SCC, composed of SA and CS, was crosslinked using $CaCl_2$ in a simple, water-based process. This environmentally friendly approach eliminates the need for synthetic polymers or toxic crosslinking agents, making it a sustainable alternative to conventional binders. The SCC demonstrated superior mechanical properties compared to SA and SC due to the incorporation of Ca^{2+} ions, which facilitated ionic crosslinking, and the presence of strong hydrogen bonding interactions. Both of these factors enhanced the structural integrity of the binder matrix and adhesion within the electrode. Electrochemical evaluations revealed that the SCC effectively accommodated Si's volumetric changes, resulting in improved cycling stability and capacity retention compared to conventional binders. This work highlights the potential of biomass-derived binders to overcome the limitations of Si anodes while promoting sustainability in battery technology.

Disclosure statement

No potential conflict of interest was reported by the author(s).

Acknowledgement

This research was supported by the National Research Foundation of Korea(NRF) grant funded by the Korea government (RS-2025-00515563) and the R&D Program for Forest Science Technology provided by the Korea Forest Service (Korea Forestry Promotion

Institute) (RS-2023-KF002435),

References

[1] Nitta N, Wu F, Lee JT, et al. Li-ion battery materials: present and future. Materials today. 2015;18(5):252-264.

[2] Van Noorden R. A better battery. Nature. 2014;507(7490):26.

[3] Armand M, Tarascon J-M. Building better batteries. nature. 2008;451(7179):652-657.

[4] Hong TH, Min W, Choi G, et al. Unified Interplay of Chemical Bond and Solid-State Kinetics in Lithium–Sulfur Batteries. Advanced Energy Materials. 2023;13(25):2300636.

[5] Lee J, Urban A, Li X, et al. Unlocking the potential of cation-disordered oxides for rechargeable lithium batteries. science. 2014;343(6170):519-522.

[6] Hong TH, Kee J, Jang H, et al. Multiphysics factor facilitating fast reaction kinetics for high-power-density Li–Se batteries. Journal of Alloys and Compounds. 2023;948:169789.

[7] Yuan T, Tan Z, Ma C, et al. Challenges of spinel Li4Ti5O12 for lithium-ion battery industrial applications. Advanced energy materials. 2017;7(12):1601625.

[8] Park I, Lee Y, Park S, et al. Microwave-mediated stabilization and carbonization of polyacrylonitrile/super-P composite: carbon anodes with high nitrogen content for lithium ion batteries. Chemistry of Materials. 2023;35(21):9182-9191.

[9] Liu Y, Shi H, Wu Z-S. Recent status, key strategies and challenging perspectives of fast-charging graphite anodes for lithium-ion batteries. Energy & Environmental Science. 2023;16(11):4834-4871.

[10] Obrovac MN, Chevrier VL. Alloy negative electrodes for Li-ion batteries. Chemical reviews. 2014;114(23):11444-11502.

[11] Wu H, Cui Y. Designing nanostructured Si anodes for high energy lithium ion batteries. Nano today. 2012;7(5):414-429.

[12] Jin Y, Zhu B, Lu Z, et al. Challenges and recent progress in the development of Si anodes for lithium-ion battery. Advanced Energy Materials. 2017;7(23):1700715.

[13] Feng K, Li M, Liu W, et al. Silicon-based anodes for lithium-ion batteries: from fundamentals to practical applications. Small. 2018;14(8):1702737.

[14] Huang W, Wang W, Wang Y, et al. Overcoming the fundamental challenge of PVDF binder use with silicon anodes with a super-molecular nano-layer. Journal of Materials Chemistry A. 2021;9(3):1541-1551.

[15] Ye R, Liu J, Tian J, et al. Novel Binder with Cross-Linking Reconfiguration Functionality for Silicon Anodes of Lithium-Ion Batteries. ACS Applied Materials & Interfaces. 2024;16(13):16820-16829.

[16] Wang H, Wei D, Zhang B, et al. Epoxy cross-linking enhanced the toughness of polysaccharides as a silicon anode binder for lithium-ion batteries. ACS Applied Materials & Interfaces. 2021;13(31):37704-37712.

[17] Wang T, Shi Z, Zhong Y, et al. Biomass-Derived Materials for Advanced Rechargeable Batteries. Small. 2024;20(45):2310907.

[18] Kovalenko I, Zdyrko B, Magasinski A, et al. A major constituent of brown algae for use in high-capacity Li-ion batteries. Science. 2011;334(6052):75-79.

[19] Mao Z, Wang R, He B, et al. Cross-Linked Sodium Alginate as A Multifunctional Binder to Achieve High-Rate and Long-Cycle Stability for Sodium-Ion Batteries. Small. 2023;19(11):2207224.

[20] Ding Y, Zhong X, Yuan C, et al. Sodium alginate binders for bivalency aqueous batteries. ACS Applied Materials & Interfaces. 2021;13(17):20681-20688.

[21] Li J, Hu X, Zhao H, et al. Cross-linked sodium alginate–sodium borate hybrid binders for high-capacity silicon anodes in lithium-ion batteries. Langmuir. 2021;38(1):402-410.

[22] Volpi N. Chondroitin sulfate safety and quality. Molecules. 2019;24(8):1447.

[23] Wu H, Yu G, Pan L, et al. Stable Li-ion battery anodes by in-situ polymerization of conducting hydrogel to conformally coat silicon nanoparticles. Nature communications. 2013;4(1):1943.

[24] Jiao X, Yuan X, Yin J, et al. Multiple network binders via dual cross-linking for silicon anodes of lithium-ion batteries. ACS Applied Energy Materials. 2021;4(9):10306-10313.

[25] Yu X, Yang H, Meng H, et al. Three-dimensional conductive gel network as an effective binder for high-performance Si electrodes in lithium-ion batteries. ACS applied materials & interfaces. 2015;7(29):15961-15967.

[26] Soury R, Jabli M, Latif S, et al. Synthesis and characterization of a new meso-tetrakis (2, 4, 6-trimethylphenyl) porphyrinto) zinc (II) supported sodium alginate gel beads for improved adsorption of methylene blue dye. International Journal of Biological Macromolecules. 2022;202:161-176.

[27] Yang K-R, Tsai M-F, Shieh C-J, et al. Ultrasonic-assisted extraction and structural characterization of chondroitin sulfate derived from jumbo squid cartilage. Foods. 2021;10(10):2363.

[28] Chen B, Xu D, Chai S, et al. Enhanced silicon anodes with robust SEI formation enabled by functional conductive binder. Advanced Functional Materials. 2024;34(34):2401794.

[29] Wang Y, Yang X, Yuan Y, et al. N-Rich Solid Electrolyte Interface Constructed In Situ Via a Binder Strategy for Highly Stable Silicon Anode. Advanced Functional Materials. 2023;33(34):2301716.

[30] Rajapaksha W, Nicholas IH, Thoradeniya T, et al. Novel alginate nanoparticles for the simultaneous delivery of iron and folate: a potential nano-drug delivery system for anaemic patients. RSC Pharmaceutics. 2024;1(2):259-271.

[31] Ma R, Feng Y, Yu J, et al. Ultralight sponge made from sodium alginate with processability and stability for efficient removal of microplastics. Environmental Science and Pollution Research. 2023;30(47):104135-104147.

[32] Senthil C, Kim S-S, Jung HY. Flame retardant high-power Li-S flexible batteries enabled by bio-macromolecular binder integrating conformal fractions. Nature communications. 2022;13(1):145.

[33] Jung HY, Jung HW, Koo MH, et al. An architecting binder derived from Antarctic red algae to accelerate sulfur redox kinetics in Li–S batteries. Materials Today. 2025;83:231-241.

[34] Zhang P, You Y, Wang C, et al. A novel anode material for lithium-ion batteries: silicon nanoparticles and graphene composite films. IOP Conference Series: Earth and Environmental Science. 2019;354(1):012079.

[35] Li Z, Wu G, Yang Y, et al. An ion-conductive grafted polymeric binder with practical loading for silicon anode with high interfacial stability in lithium-Ion batteries. Advanced Energy Materials. 2022;12(29):2201197.

[36] Li Y, Yan K, Lee H-W, et al. Growth of conformal graphene cages on micrometre-sized silicon particles as stable battery anodes. Nature Energy. 2016;1(2):1-9.

[37] Wang F, Wang Y, Liu Z, et al. Carbon-Binder Design for Robust Electrode–Electrolyte Interfaces to Enable High-Performance Microsized-Silicon Anode for Batteries. Advanced Energy Materials. 2023;13(40):2301456.

[38] Hong TH, Kim JD, Kang W, et al. Operational strategy for multiredox-reaction electrodes for long-lifespan Na-ion hybrid capacitors. Chemical Engineering Journal. 2023;475:146132.

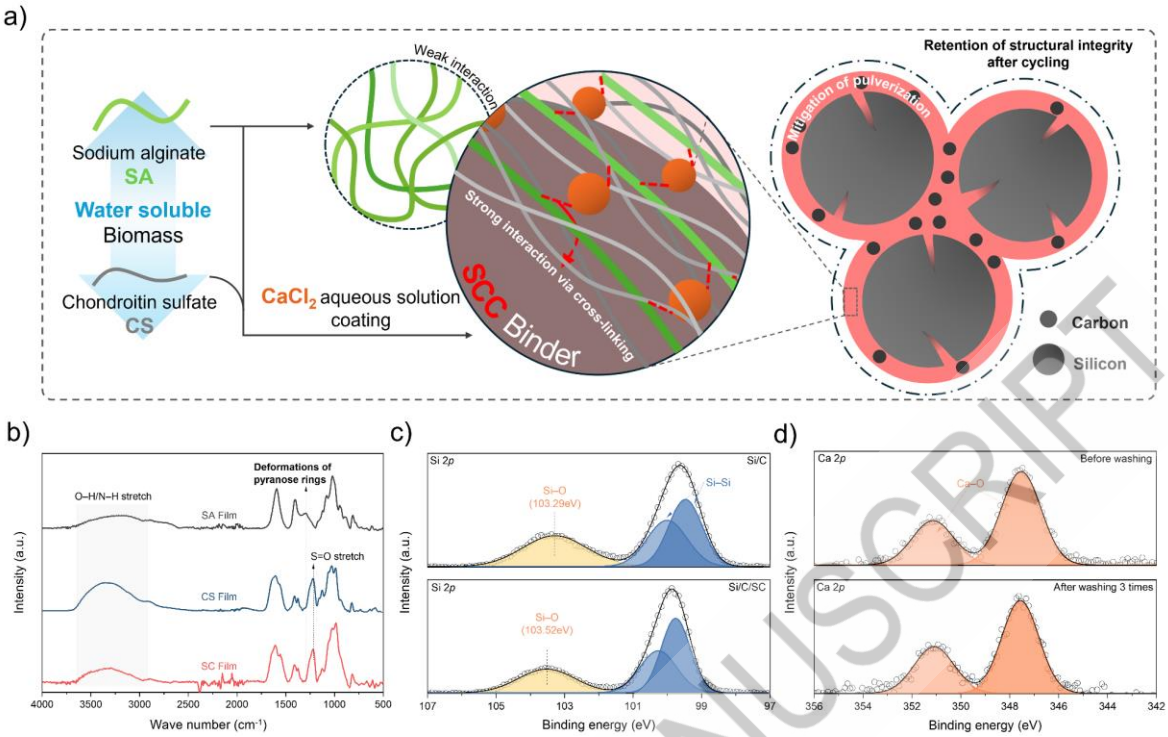

Figure 1. (a) Schematic illustration of the fabrication process of the SCC and its integration into the electrode structure. (b) FT-IR spectroscopy profiles of SA, CS, and SC films. (c) Si 2*p* XPS Spectra of Si/C and Si/C/SC mixed powders. (d) Ca 2*p* XPS Spectra of the SCC/Si before and after ethanol washing.

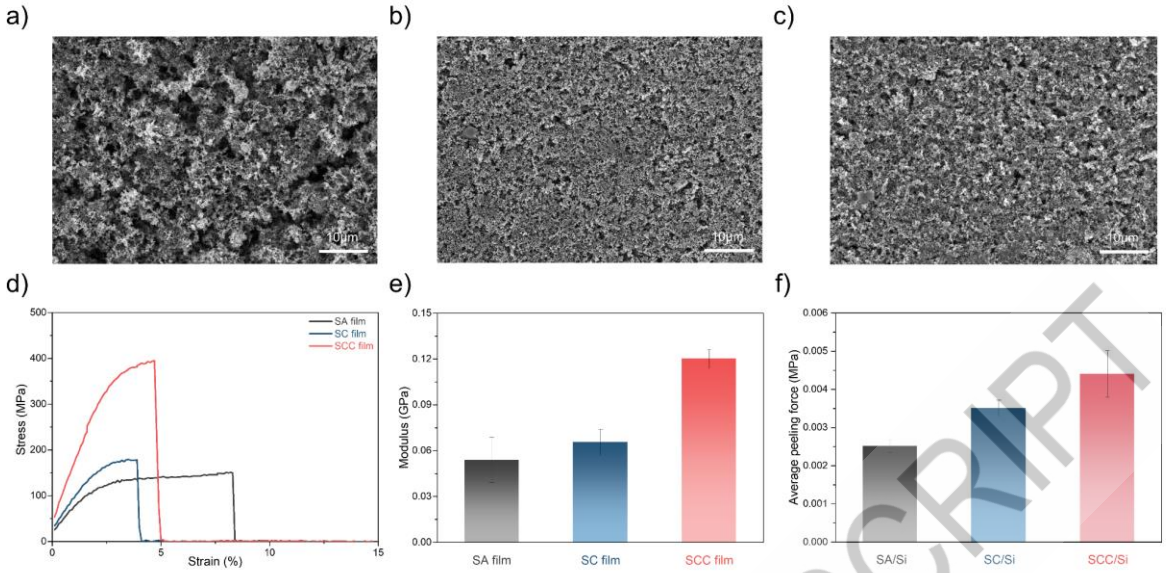

Figure 2. Top-view SEM images of electrodes with different binders, with (a) SA, (b) SC, and (c) SCC. Tensile strength measurement of pure binder films, with (d) stress-strain (SS) curves and (e) Young's modulus derived from the data. (f) Average peeling force of electrodes with different binders.

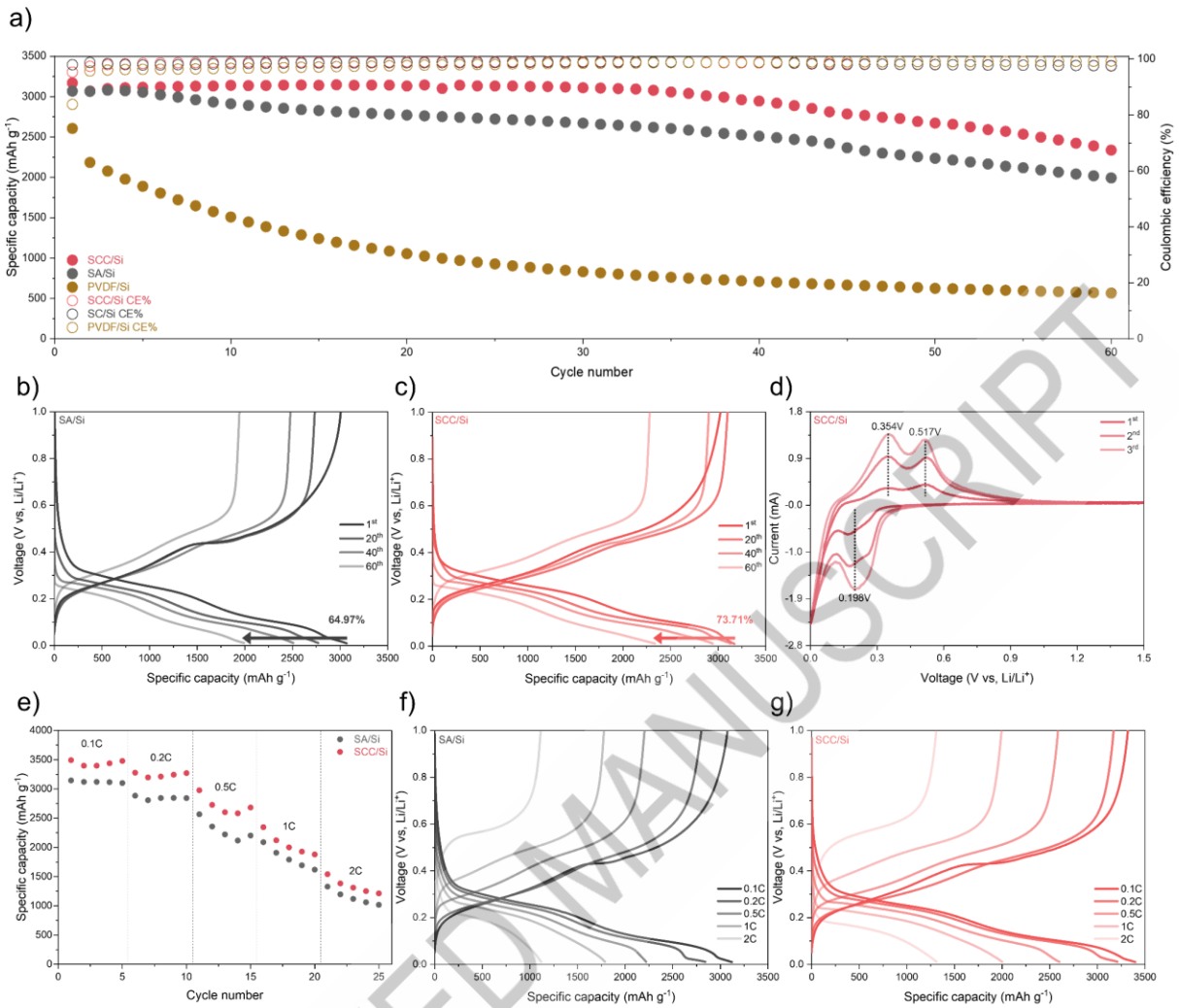

Figure 3. (a) Cycling data of PVDF/Si, SA/Si, and SCC/Si at a 0.2C rate, with GCD profiles of (b) SA/Si and (c) SCC/Si, derived from this data. (d) CV profile of the SCC/Si. (e) Capacity data measured at increasing current densities from 0.1C to 2C. GCD profiles of (f) SA/Si and (g) SCC/Si, derived from the rate data.

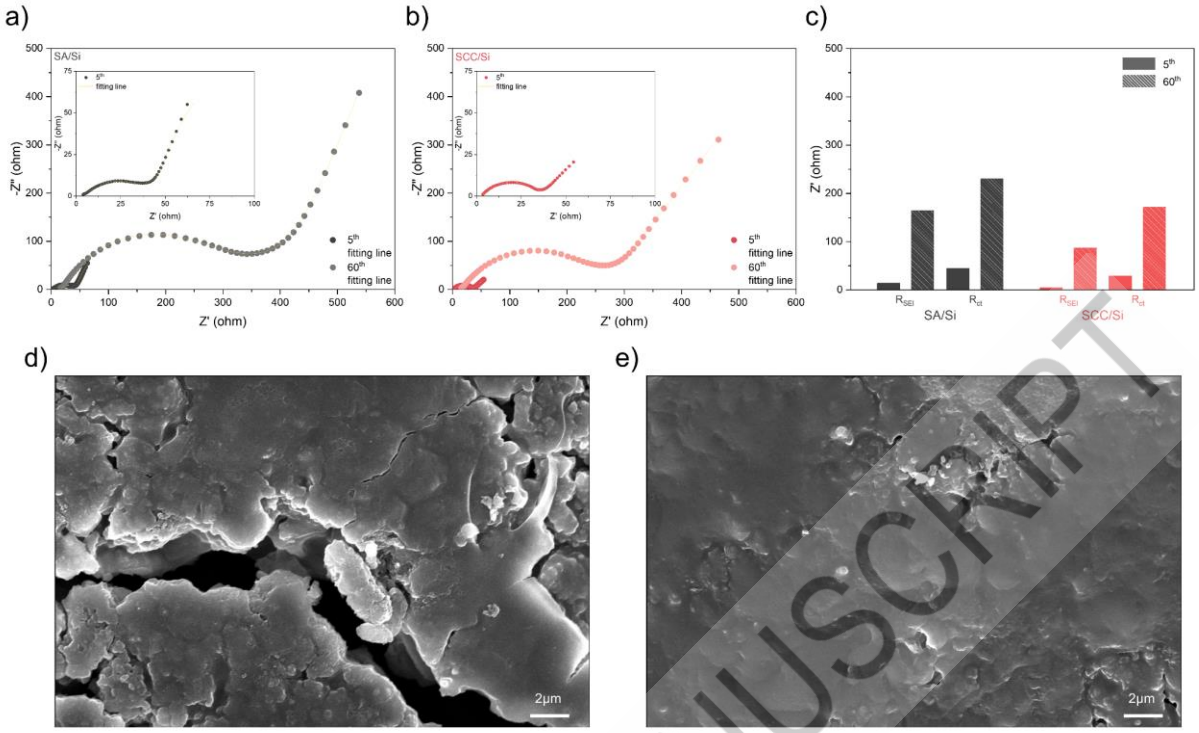

Figure 4. Nyquist plots from EIS measurements after the 5th and 60th cycles for (a) SA/Si and (b) SCC/Si. (c) R_{SEI} and R_{ct} values derived from Nyquist plots after the 5th and 60th cycles. Top-view SEM images of post-cycled (d) SA/Si and (e) SCC/Si.

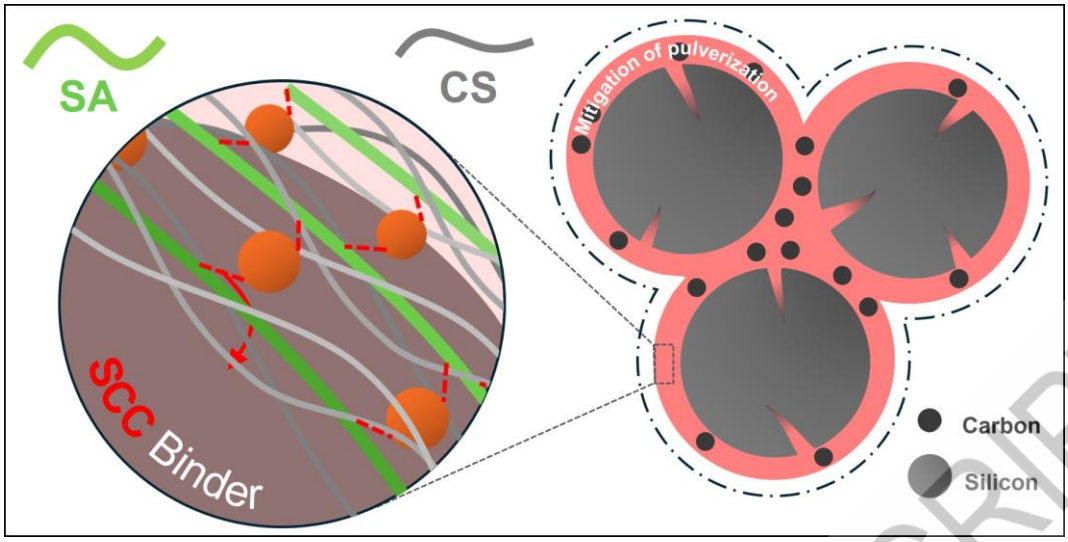

GraphicalAbstract1

Statement of Novelty

This study presents a sustainable binder for silicon anodes, demonstrating enhanced mechanical strength, structural integrity and electrochemical stability, addressing volumetric expansion and advancing eco-friendly lithium-ion battery technologies.

Supplementary materials

Sustainable and Robust Biomass-Based Binder for Silicon Anodes in Lithium-Ion Batteries: Cross-linked Sodium Alginate and Chondroitin Sulfate

Hyun Wook Jung [a,1], *Seung Min Ko* [a,1] *and Jung Tae Lee* [a,*]

[a] Department of Convergent Biotechnology and Advanced Materials Science, Kyung Hee University, 1732, Deogyeong-daero, Giheung-gu, Yongin-si, Gyeonggi-do, 17104, Republic of Korea

* Corresponding authors

E-mail addresses: J.T.Lee (jungtae@khu.ac.kr)

[1] These authors contributed equally to this work

Keywords: Silicon anode, cross-linking, binder, eco-friendly, biomass

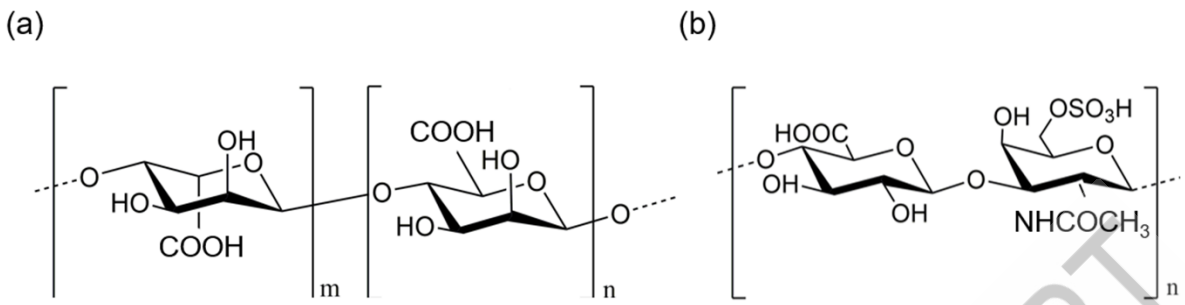

Figure S1. Chemical structures of (a) sodium alginate (SA) and (b) chondroitin sulfate (CS)

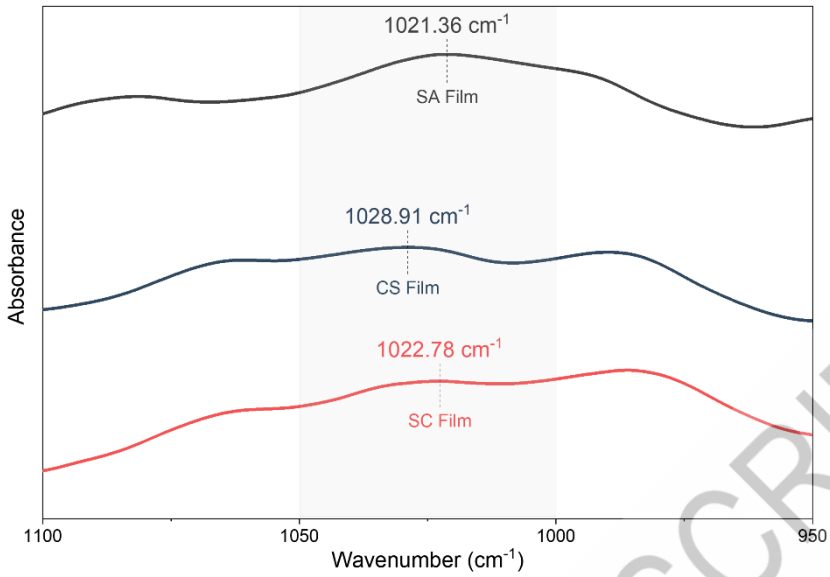

Figure S2. FT-IR spectroscopy profiles of SA, CS, and SC films in the wavenumber range from 1100 cm^{-1} to 950 cm^{-1}.

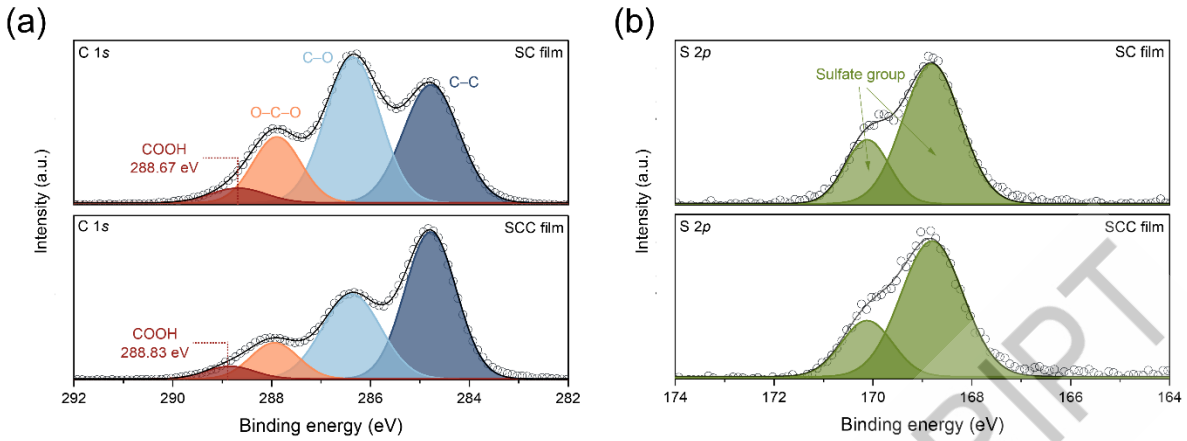

Figure S3. C 1*s* and S 2*p* XPS Spectra of SC and SCC Films.

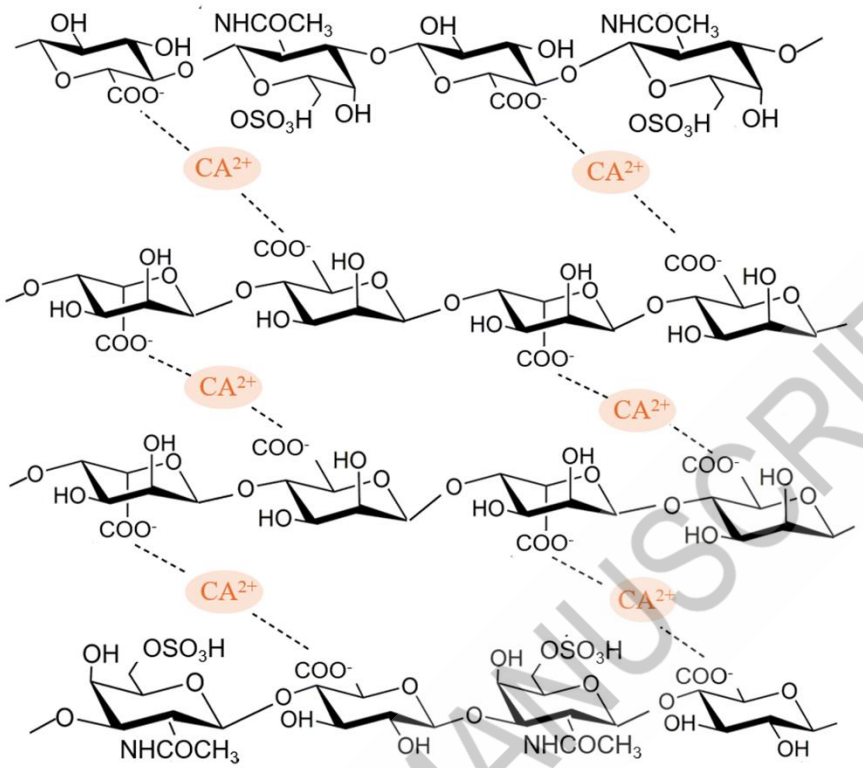

Figure S4. Schematic illustration of the chemical structures of SCC.

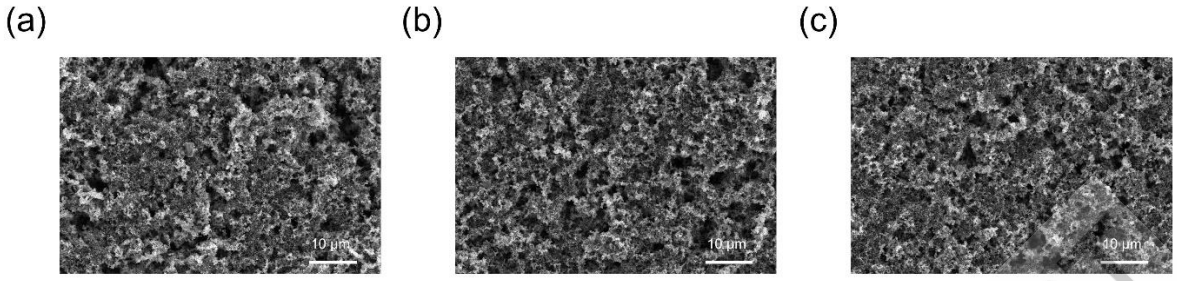

Figure S5. Top view SEM images of electrodes prepared with varying SA to CS ratios; (a) represents a 5:1 ratio, (b) a 1:1 ratio, and (c) a 1:5 ratio.

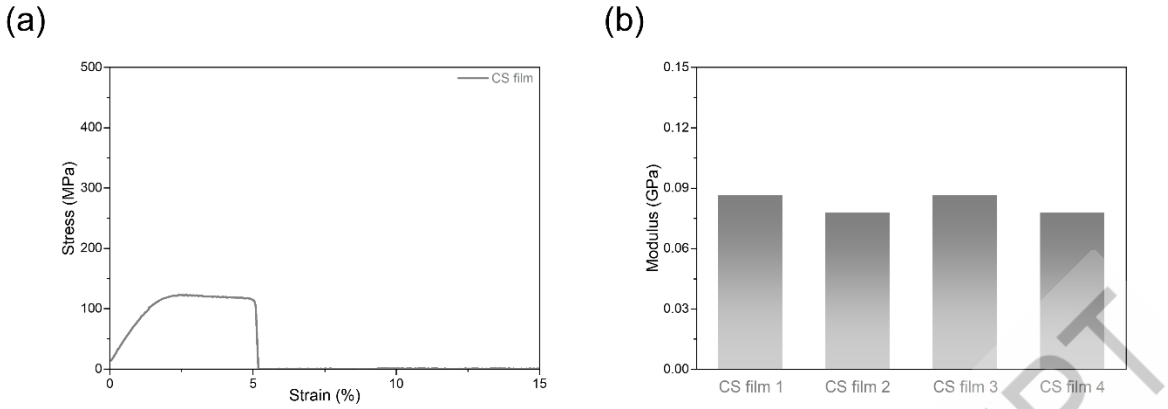

Figure S6. Tensile strength measurement of pure CS film, with (a) stress-strain (SS) curves and (b) Young's modulus values derived from the tensile strength measurements of various CS films; the average value is 0.082 GPa with a standard deviation of 0.0049.

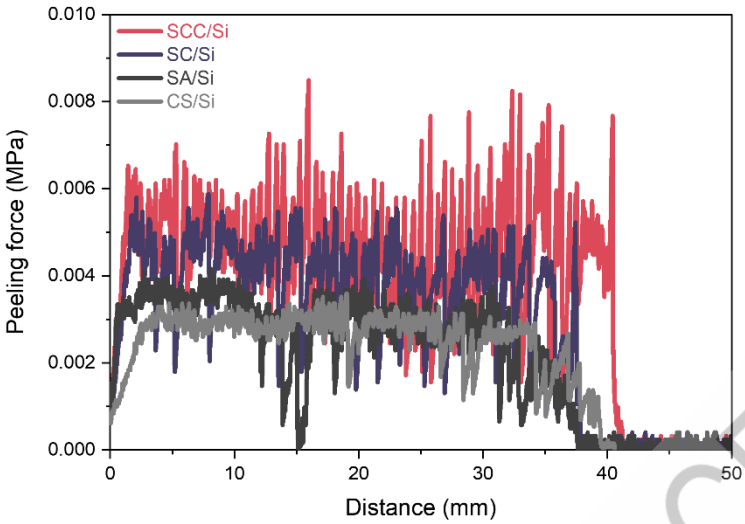

Figure S7. Peeling test results of SA/Si, SC/Si, CS/Si and SCC/Si.

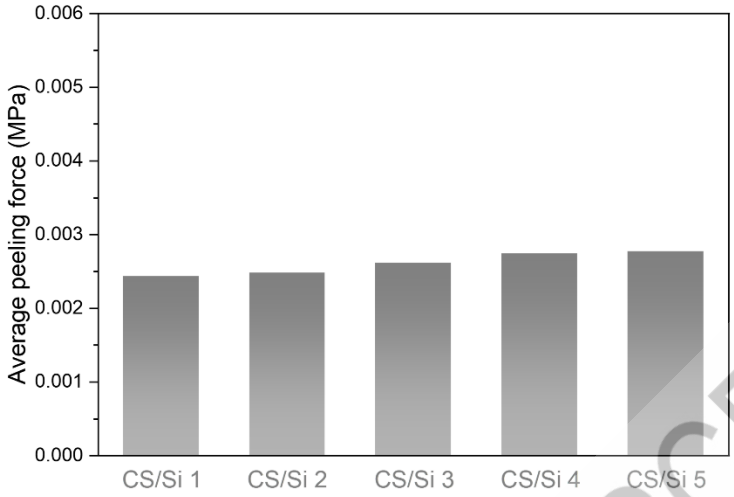

Figure S8. Average peeling force of CS/Si; the average value is 0.00254 MPa with a standard deviation of 0.0002.

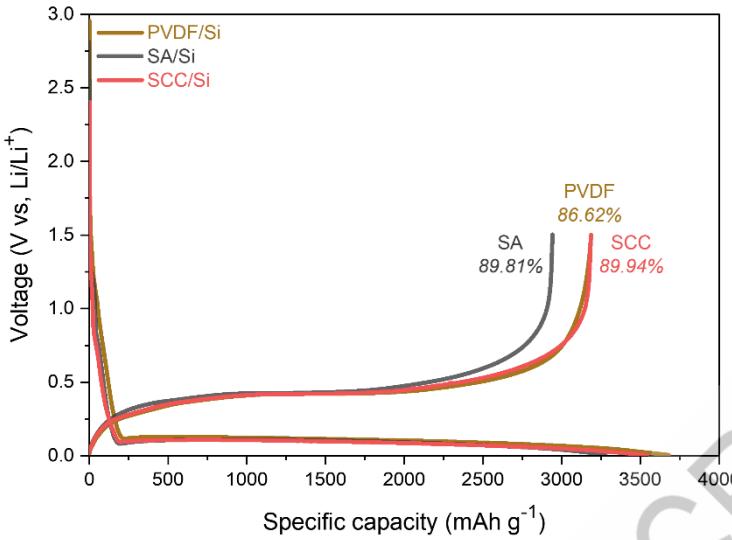

Figure S9. GCD profiles and initial coulombic efficiency values derived from 0.2C Cycling data of PVDF/Si, SA/Si, and SC/Si.

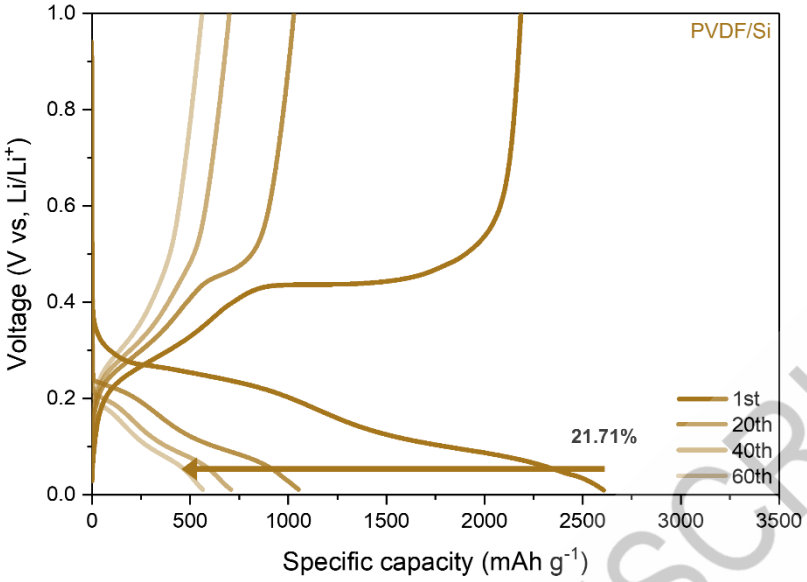

Figure S10. GCD profiles of the PVDF/Si extracted from 0.2C cycle data.

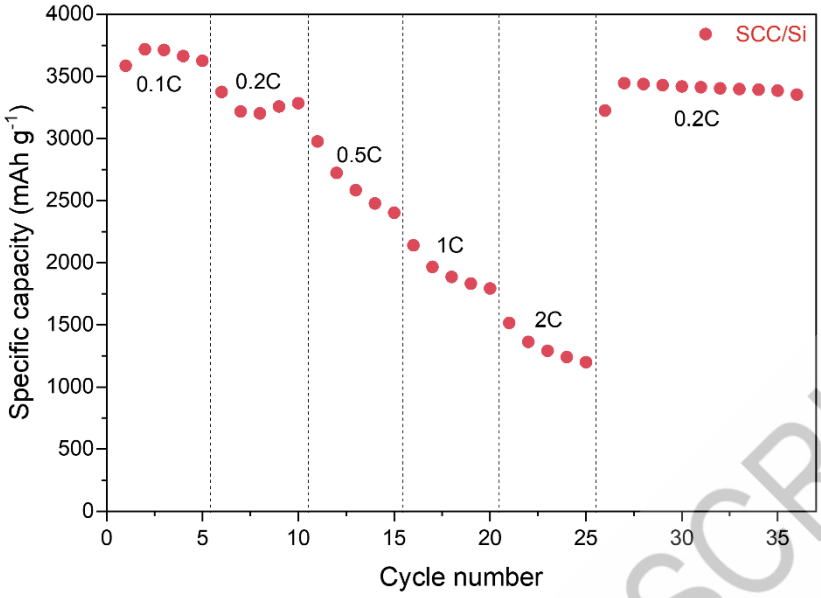

Figure S11. Capacity data measured of SCC/Si at increasing current densities from 0.1C to 2C and during the return to 0.2C rate.

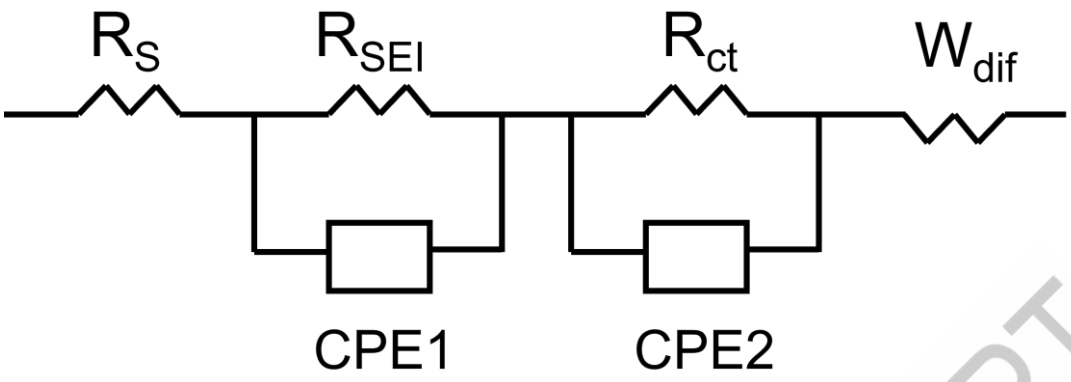

Figure S12. EIS circuit adopted for deriving each resistance value in the nyquist plot.